The 9th European Congress on Computational Methods in Applied Sciences and Engineering
ECCOMAS Congress 2024
3–7 June 2024, Lisboa, Portugal

AUTOMATED FLOW PHYSICS IDENTIFICATION AND CLASSIFICATION IN MULTIPHYSICS MULTIFIDELITY SIMULATIONS

Ahmed A. Sheikh Al-Shabab[1], Paulo A. S. F. Silva, Panagiotis Tsoutsanis[1], and Martin Skote[1]

[1] School of Aerospace, Transport and Manufacturing, Cranfield University,
College Road, Cranfield, Bedfordshire, MK43 0AL, UK
Corresponding Author: A.A.Sheikh-Al-Shabab@Cranfield.ac.uk

Key words: Multiphysics, Multifidelity, Turbulent Flow, Shock Absorbers

Summary. Advances in computational modelling and the steady rise in computational power availability are driving interest in increasingly complex multiphysics simulations. These simulations can potentially provide valuable insights into the dynamics of poorly understood systems and enable ambitious technological advances through accounting for the dominant flow physics under a wider range of operational conditions. Nevertheless, the identification and classification of flow phenomena are central to the viability of such a framework, as they enable efficient use of the available resources in a numerically robust manner. Furthermore, the correct classification of cases based on common underlying flow physics can support algorithm training and improve machine learning predictive accuracy within each group. This is explored in the present work in the context of oleo-pneumatic shock absorbers with a focus on the multiphysics interaction between hydraulic oil and gas. Metrics for the interaction are introduced and their suitability is discussed in the wider context of shock absorber flows.

1 Introduction

The integration of multiphysics simulations into design and database generation workflows has been regularly cited as a key challenge in the future development of Computational Fluid Dynamics (CFD) (1; 2). The difficulty doesn't only include the development of accurate physical models, but also extends to handling the automation of pre and post-processing workflows, improving algorithm stability, and managing large datasets efficiently (1; 3). Furthermore, some applications present additional challenges in the lack of reliable validation data, uncertainty in the initial conditions, and unsteady boundary conditions. Examples of such applications include extraterrestrial flows, nuclear reactions, and aircraft oleo-pneumatic shock absorber flows, among others.

While the workflow presented in the current study can be generally utilised in different applications, the practical examples presented and discussed here will focus on the simulation of oleo-pneumatic shock absorbers. Shock absorber simulations are challenging due to many of the points discussed above, especially the wide range of flow physics involved, lack of validation data, and complex geometries (4; 5).

The long term objective is to develop workflows that facilitate the automation of flow physics identification and case classification depending on the significance of detected flow phenomena. However, for such a framework to be possible, suitable flow metrics need to be identified in order to accurately detect and measure the flow physics of interest. Dedicated studies at a range of fidelity levels have been conducted to provide the building blocks necessary for such a framework. These include scale resolving simulations of the orifice nearfield (6), unsteady multiphase mixing simulation of a drop test (7), and a two equation dynamic system model to simulate the shock absorber system (8), where the dynamic system model is based on the work by Milwitzky and Cook (9). The present work explores bringing these different simulations together into a multifidelity framework facilitating efficient design space exploration and database generation. In order to achieve this, the analysis and discussion will focus on some examples of flow metrics that are being developed and their relevance within the context of oleo-pneumatic shock absorber flows.

2 Methodology

The methodology section will mainly focus on the overall workflow development around the various simulation types, rather than provide the details of each fidelity level setup and numerical methods. These details can be found the respective publications covering the specific simulation in question, covering single phase

scale resolving simulation of the orifice nearfield (6), multiphase unsteady mixing based on a practical loading profile (7), and two-equation dynamic system model for low-fidelity performance prediction and for unsteady boundary condition generation (8; 9).

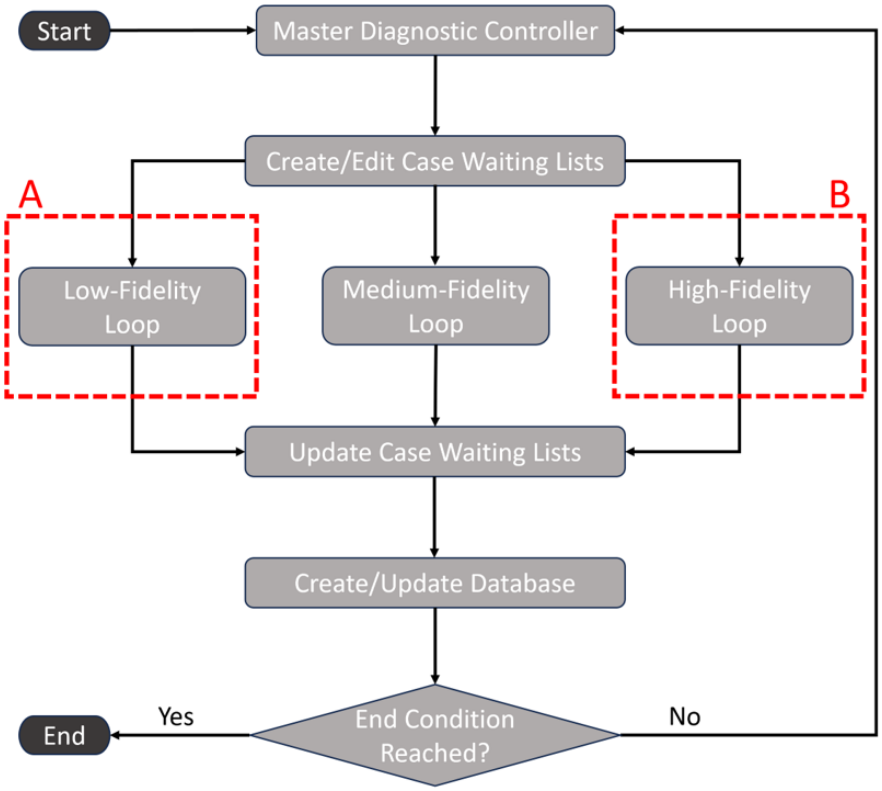

Figure 1: Overall multi-fidelity loop flowchart

The proposed top level multi-fidelity workflow is illustrated in Fig. 1. An overall *master diagnostic controller* runs in the background of the framework and monitors the progress of simulations and their outcomes. It facilitates flexible supervision and adaptive control of simulations. This *master controller* is tasked with many tasks including:

- monitoring resource utilization.
- coordinate multi-fidelity simulations.
- search and assess whether a requested case is present in the existing database or requires a dedicated simulation.
- assessing convergence and adjusting the numerical parameters of cases that diverge or fail to meet convergence criteria.
- run diagnostic tool to identify and classify flow physics on the fly or after the end of simulations.
- initiate post-processing analysis streams.
- lower-fidelity model tuning based on the latest available data from higher-fidelity simulations.
- archive completed cases in a database.
- conduct design space exploration or optimization exercises depending on the objectives.

This provides a flexible architecture to maximize computational resource usage for efficient design space exploration. The customised features of the diagnostic tool are launched with their respective fidelity level

simulation or analysis. The modularity of the framework is central to the overall architecture, as it facilitates expanding the simulation types and the post-processing analysis as required, based on the available output.

Interactions between fidelity levels are facilitated through priority-based queues. Low-fidelity components can request higher-fidelity calibration data by submitting cases to their queues with low initial priority. This avoids dictating resource usage. Low-fidelity cases may run without full calibration initially to provide baseline solutions when higher-fidelity references are unavailable. These can also be used in sensitivity studies to identify the parameters that hold a higher potential impact during the tuning process.

It is worth clarifying the type of simulations and analysis that falls under each of the low, medium and high simulation fidelity levels, in the context of the present work:

- **Low Fidelity:** One dimensional system level simulations that are based on algebraic laws derived from empirical or analytical theories, with simulations lasting in the order of seconds generating results of mainly integral parameters that lack geometrical field detail.
- **Medium Fidelity:** Two dimensional, (mainly) steady state simulations that are able to provide some field information, for example regarding turbulence properties, with simulations lasting from minutes to a few hours and generating two dimensional, potentially transient, field data for post-processing.
- **High Fidelity:** Two or Three dimensional time accurate simulations that include multi-physics or dynamic mesh capability, with a run time of hours to days and generating transient and averaged field data for post-processing.

Dedicated workflow diagrams are implemented for the pre-processing, simulation, and post-processing logic at each fidelity level as marked with A and B on Fig. 1 . This enhances customizability and encapsulates steps specific to each model in a modular fashion. Standardized CSV-format waiting list files are generated for pending cases, with columns for tracking attributes such as case ID, parameters, priority tier, and requesting solver.

Descriptive naming conventions facilitate searching lists and the results database to identify specific cases. Standard data formats such as VTK enable efficient sharing of case data between fidelity levels for model calibration, unsteady boundary conditions, and future algorithm training activities.

In summary, the modular framework architecture, structured case tracking, priority-based scheduling, and data sharing capabilities provide a robust platform for automated efficient exploration of the design space across interfaced fidelity levels.

Figure 2 shows an expanded versions of the low and high-fidelity loops shown in Fig. 1. Each fidelity level can have a customized workflow that fits into the overall framework, allowing flexibility in the tools and techniques used at each level. Although three fidelity levels are shown in the present loop, the modular structure facilitates the addition of extra solver loops, by customising only the information interface between the new solver and the main loop to ensure consistency with existing database entries.

A key point to address is the validation of the simulations being conducted at the various fidelity levels. As mentioned previously, the lack of data and standard geometries is a challenge when conducting oleo-pneumatic shock absorber simulations. The strategy adopted here is to use the limited available drop test data, such as the study of Miltwitzky and Cook (9), to validate the initial simulation setup, and to test different strategies for geometry simplifications, gird design and accounting for the unsteady boundary conditions. The the modular structure facilitates validation through running the same case on a number of fluid solvers with different numerical methods, to assess the accuracy and errors in cases which lack any validation data availability.

2.1 Validation Case

Most simulation data presented in the present work is based on the drop test case investigated by Milwitzky and Cook (9), as they provide experimental measurement of a drop test for an oleo-pneumatic shock absorber of a small military trainer aircraft. The drop test shock absorber geometry is slightly simplified by removing the metering pin in the operational shock absorber leading to produce a constant orifice diameter shock absorber. Although not all the geometrical details are provided, the key parameters available in Milwitzky and Cook (9) enable an approximate reconstruction of the internal shock absorber geometry, with the aid of general sizing guidelines from the standard landing gear publications, such as Currey (4). The main details of the drop test are listed in Table 1.

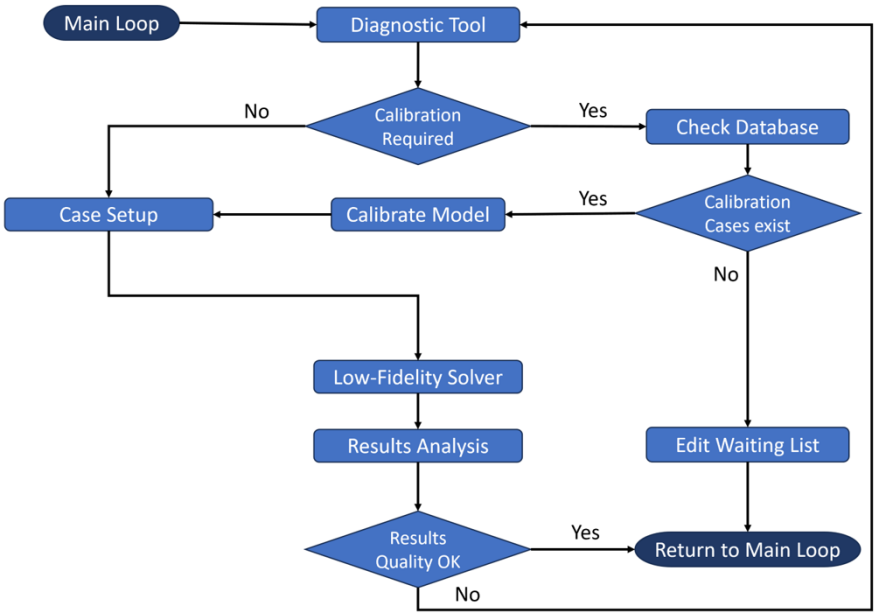

(a) Low-fidelity example

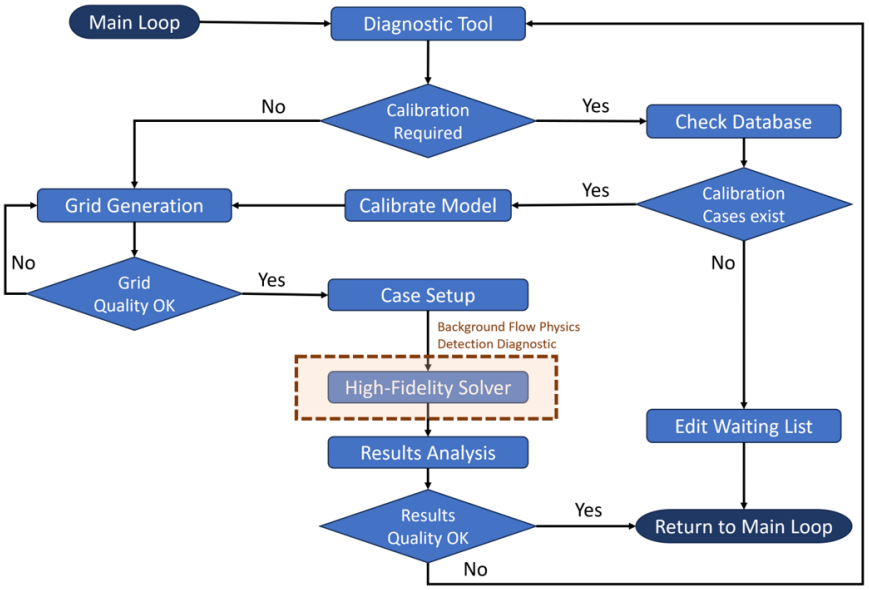

(b) High-fidelity example

Figure 2: Inner solver loop flowchart

The simplified shock absorber geometry used in the present investigation is demonstrated in Fig. 3. The fixed diameter orifice plate provides the hydraulic resistance that dissipates the majority of the vertical kinetic energy at impact (9; 4). The importance of the hydraulic resistance in shock absorber performance motivated a closer study of the orifice nearfield vicinity (6), where the turbulent development of the shear layer downstream of the orifice tip was investigated. The developing turbulent flow was validated against standard shear layer spreading rate results and approximate self-similarity profiles available in the literature, to compensate for the lack of validation data (6). In addition, a preliminary design study of the impact of different orifice designs was conducted to test the sensitivity of performance metrics to orifice shape parameters (10).

A main challenge of shock absorber simulation is in handling the inherent time dependence of the domain boundary conditions, which effectively drive the flow according to the applied loading profile. This unsteady boundary case is one of the key challenges often cited in the future development of CFD (2). There are two main options to model the flow inside the shock absorber as it becomes compressed by the telescoping lower wall motion due to an impact. The first is to use a moving mesh algorithm, which allows the physical extent of the computational domain to change with time in accordance with the stroke rate of the shock absorber for a given

Working Fluid type (Oil/Gas)	AN-VV-O-366B / Air
Hydraulic Oil Density, ρ_h (kg/m^3)	869
Polytropic Constant, n	1.12
Orifice discharge Coefficient, C_d	0.09
Upper Mass, M_U (kg)	1090
Lower Mass, M_L (kg)	59.4
Vertical Velocity at Initial Contact, V_0 (m/sec)	2.70
Gravitational Acceleration, g (m/sec^2)	9.81
Pneumatic Area, A_a (m^2)	5.35×10^{-3}
Hydraulic Area, A_h (m^2)	4.37×10^{-3}
Orifice Area, A_o (m^2)	5.19×10^{-5}
Initial Gas Volume, v_0 (m^3)	1.00×10^{-3}
Initial Gas Pressure, p_{a0} (bar)	3.00
Tire Diameter, d (m)	6.86×10^{-1}

Table 1: Landing gear drop down test summary

disturbance. However, this method can lead to degraded mesh quality in critical areas of the computational domain and could add significant computational expense to the overall case. On the other hand, it is possible to simulate the shock absorber stroke using a static mesh with a variable inlet velocity profile that applies the required loading to the shock absorber. This has the advantage of allowing better control over grid quality and being more robust when different loading profiles are used, although it does add some mass into the system (hydraulic oil) to achieve the required loading profile. The second approach is adopted in the present study.

Another challenging aspect of shock absorber multiphase simulations is that the location and shape of the gas–oil interface changes significantly during the simulation; hence, either an adaptive meshing technique or a very fine grid must be used to allow the flow development to be captured accurately. Both of these options add to the cost of simulations. Hence, it is decided, as a compromise, to use a relatively fine upper chamber grid, as shown in Fig. 3c, and a 2D axisymmetric boundary condition rather than a full 3D simulation.

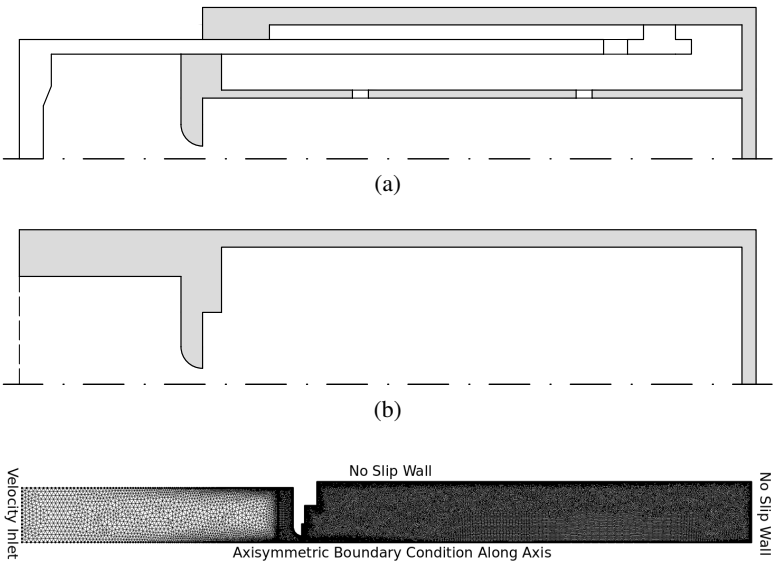

Figure 3: Shock absorber geometry simplification: (**a**) telescoping internal geometry; (**b**) fixed shock absorber geometry; (**c**) unstructured mesh used with boundary conditions.

A low-fidelity two-equation dynamic system solver is developed and validated (8) to provide realistic boundary conditions for the high-fidelity simulations investigating multiphase mixing in shock absorbers (7; 10). The boundary conditions used in these simulations are also illustrated on Fig. 3c, with an unsteady velocity inlet profile corresponding to the piston stroke velocity, as calculated using the dynamic system model. The mass-spring-damper system used to represent the shock absorber is illustrated in Fig. 4a, with the calculated piston

velocity profile plotted in Fig. 4b.

It is worth clarifying that the high-fidelity simulations start when the shock absorber stroke rate becomes non-zero in Fig. 4b, as the two-equation dynamic system model includes the effect of tyre deflection (9), which delays the response of the shock absorber slightly before it starts compressing. In addition, the streamwise direction in these simulations is along the horizontal x-direction with the corresponding velocity component and turbulence components, while the vertical y-direction corresponds to the radial direction inside the shock absorber.

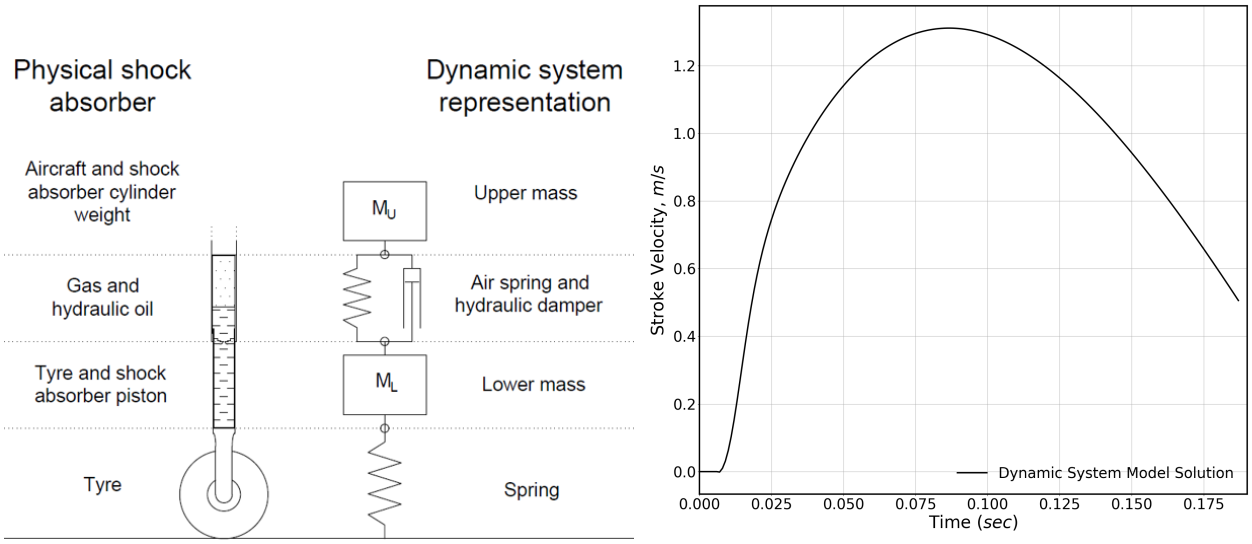

(a) Time spectrum at a point in mixing layer.

(b) Spacial spectrum over a box.

Figure 4: Shock absorber geometry and some setup details: (a) dynamic system model; (b) stroke rate profile calculated from the 2-DOF dynamic system model.

Both structured and unstructured grids were tested, with each offering some advantages. The focus on automation and support of complex geometries led to more focus on unstructured grids in the present workflow development, with the grid illustrated in Fig. 3c, being typical. Grid convergence studies were conducted, with the details provided in the respective publications (7; 10). In unsteady multiphase mixing cases, the Menter SST RANS model (11) is used , which is an aerospace standard model that has been extensively used and validated (11). It has also been successfully used in free shear flow applications, and in cases with shear layer deflection in the nearfield, such as open jet wind tunnels (12; 13).

3 Results and Discussion

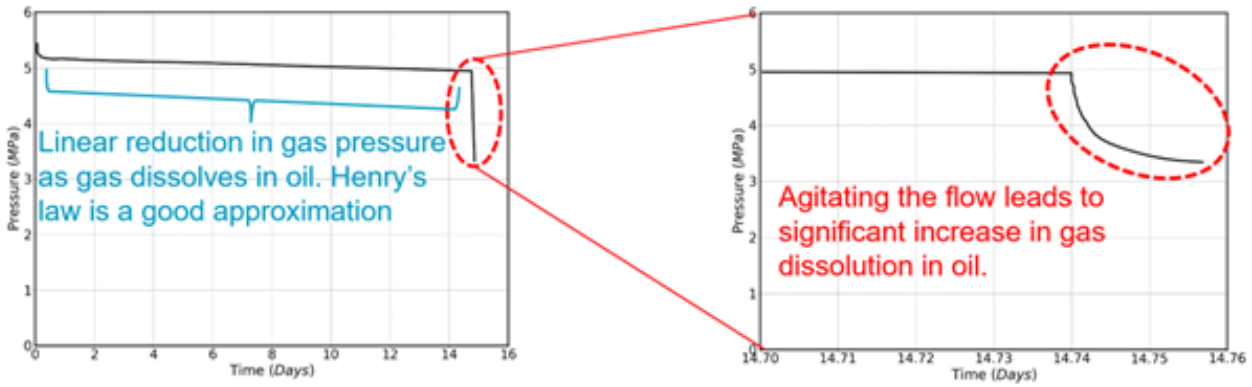

Figure 5: Gas dissolution into hydraulic oil in a pressure tank. Agitation applied after two weeks. Data values from Schmidt (5)

The discussion in this section will focus on considerations related to the prediction of gas pressure available inside the shock absorber, as this will serve as a useful demonstration of the challenges involved and the potential indicators that can be used by the diagnostic tool to predict the gas pressure available under different conditions. This will lead to discussion of gas dissolution in oil, then discussion of the effort to quantify the severity of mixing between the oil and gas to assess the level of agitation due to its influence on dissolution. Finally, cavitation monitors are briefly discussed and the likely impact of dissolution on cavitation.

Estimating gas dissolution in hydraulic oil under a given pressure is an important, yet challenging, consideration in shock absorbers. The rate and magnitude of this effect is heavily dependent on environmental factors and the contact area to depth ratio of the shock absorber design, in addition to the unknown initial conditions of the oil's existing gas content. These factors determine the time required to reach equilibrium between the two phases under a given pressure and temperature. Figure 5 is adapted from Schmidt (5), showing the rate of dissolution of gas into oil in a pressure tank initially under static condition for the first 14 days. The approximately straight line is in good agreement with Henry's law for dissolution, Eq. 1. However, when some agitation is introduced into the system, the rate of dissolution of gas increases dramatically.

$$C_{Gas} = kP_{Gas} \tag{1}$$

where, C_{Gas} is the gas concentration, k is a constant and P_{Gas} is the partial pressure of gas.

The increase in dissolution under agitation seen in Fig. 5 is important in shock absorber geometries that allow direct contact between oil and gas, as in the case of Milwitzky and Cook (9). That is because aggressive mixing due to landing can lead to a significant reduction in gas pressure. Furthermore, the mixing can change the nature of oil compression from an isentropic relation to a polytropic one under the influence of oil cooling the gas during the rapid compression in a drop test or landing. Figure 6 shows the different compression curve and the significant change in stroke position that corresponds to a given pressure under each compression relation. The differences become more pronounced at high pressure values due to the exponent impact at higher values, making the difference between these assumptions larger. These consideration must be studied to avoid shock absorber bottoming and internal components coming into contact under some loading profiles.

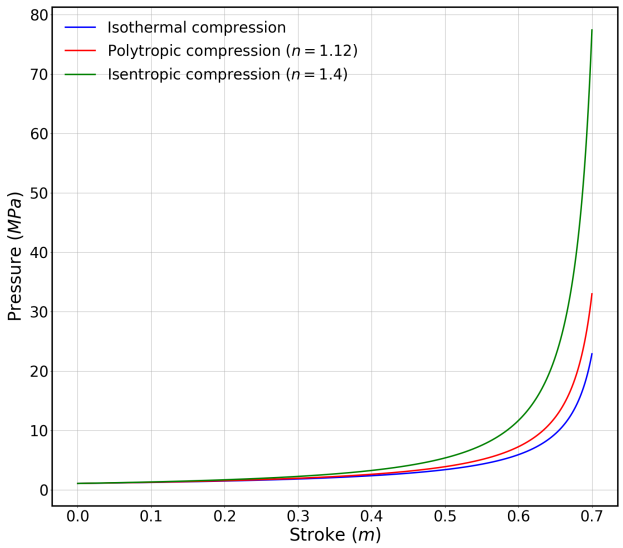

Figure 6: Gas compression curves under the isothermal, isentropic and polytropic assumptions.

Multiphase mixing between hydraulic oil and gas at an advanced stage of the shock absorber stroke is visualised in Fig. 7. The complexity of the interaction between the oil and gas highlights the need for a quantitative approach to systematically assess the multiphase mixing as the stroke progresses from a straight line interface initially, shown in Fig. 7a, advancing towards its full complexity as the gas bubble breaks into smaller ones. Slightly different variations in a mixing quality parameter were proposed in the literature to quantify mixing processes (14; 15; 16). A similar idea is implemented here, where the mixing index (MI) in the present study, defined according to Equation (2), is used to isolate the interface between the two phases at a

specific volume fraction value, taken to be $\alpha = 0.5$ in all MI analyses presented.

$$MI_T = \Sigma((1 - \sqrt{(2\alpha - 1)^2}) * A_{Cell}) \tag{2}$$

where the MI has a value of 1.0 when $\alpha = 0.5$, indicating an interface cell, while $MI = 0$ when $\alpha = 0$ or 1, corresponding to a cell with only a single phase. The utility of the MI as a method of isolating the interface between the phases is demonstrated in Fig. 7b, where it clearly captures the developing complexity of the interaction. Furthermore, a measure of the interface area (length in 2D) can be obtained by multiplying the MI value by the local cell area (per unit depth in 2D simulations).

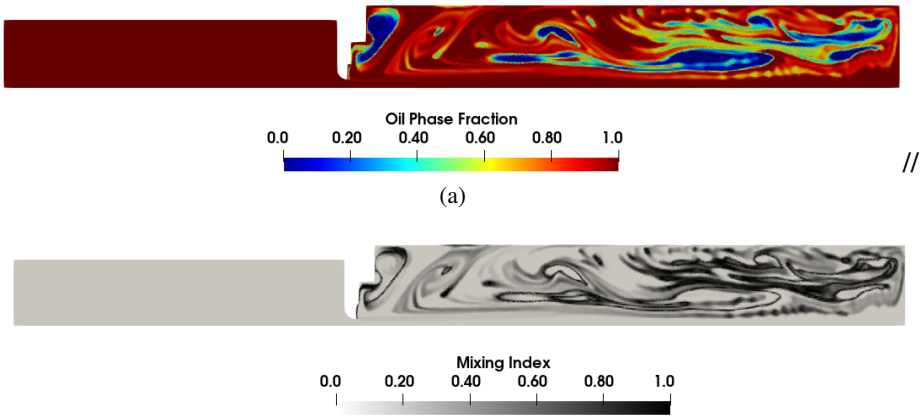

(a) (b)

Figure 7: Multiphase contour plots demonstrating how the mixing index can be applied to visualise the interface cells in order to quantify the mixing intensity at $t = 0.129$ $sec.$ (**a**) Oil phase fraction; (**b**) Phase interface.

The interface area between the two phases corresponding to the drop test case is plotted in Fig. 8a. The initial value is zero because the initialisation of the two phases splits the domain into two perfectly defined regions ($\alpha = 0$ or $\alpha = 1$) with an instantaneous transition between the oil and gas phases. However, the full range of α values develops immediately after the simulation begins. A few distinctive stages of the phase mixing process can be identified and linked with the field development seen in the contour plots of Fig. 7 a:

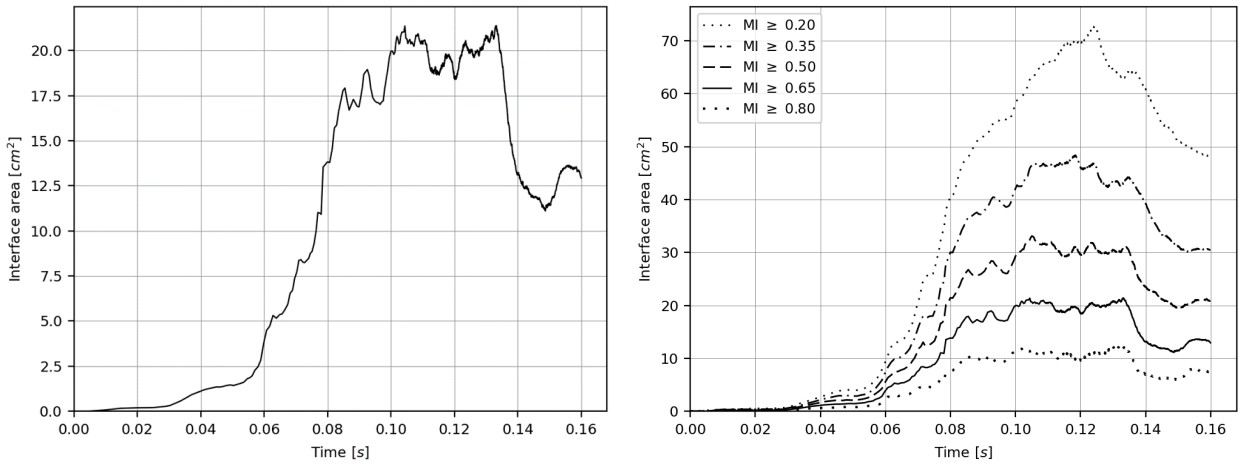

(a) (b)

Figure 8: Mixing index plots (**a**) Multiphase interface time history demonstrating the different stages of mixing and the sharp gradients that indicate the occurrence of strong mixing.; (**b**) Sensitivity of mixing index to the cutoff value used to designate boundary cells.

- Initial slow increase in interface area while the gas remains mainly in a single bubble, which continues until approximately t = 0.06 s in the present drop test simulation;

- A sharp increase in interface area after the main bubble starts breaking up into smaller ones over the highest stroke rate values between t = 0.06 s and t = 0.1 s;
- An approximate plateau of fluctuating values around a roughly steady interface area value, extending from t = 0.1 s to t = 0.135 s;
- A sharp decrease in interface area towards the end of the stroke, beyond t = 0.135 s, probably caused by the agglomeration of the gas into larger bubbles as the stroke rate decreases and the flow begins to settle again.

In calculating the mixing index, MI, a practical decision has to be made regarding the cutoff MI value taken to signify a boundary cell. The cutoff value used in Fig. 8a is ($MI \geq 0.6$), however, a range of alternative values were tested and plotted in Fig. 8b. Using a lower cutoff value increases the impact of cells with a smaller phase mixing ratio, i.e. increases the sensitivity to cells with very high or very low phase fraction values. This increased sensitivity is particularly significant during strong mixing around the second half of the stoke, when the main gas bubble breaks up and causing a wider dispersion of smaller gas bubbles. While the impact of cutoff value choice is less pronounced during the early stroke stages when the gas is still concentrated in a single large bubble.

Cavitation is another phenomenon of interest linked to the pressure field, in which the dissolved gas can form bubbles in low pressure regions. It occurs when the static pressure falls below a critical threshold, depending on the type of cavitation (17; 18), leading to the formation of incipient gas bubbles that grow in low pressure regions and are then convected to higher-pressure regions, where they could violently collapse, leading to the formation of shock waves that apply high stresses on nearby surfaces. Thus, cavitation often adversely impacts the operational life span of internal components. While cavitation modelling is beyond the scope of the present work, it is possible to monitor the potential for its occurrence and to identify the regions that are most susceptible to it. Probes are placed along the orifice exit line and along the axis of symmetry, as marked in Fig. 9, to assist in monitoring the flow parameters in the vicinity of the orifice over the stroke duration. Uniformly distributed probes are placed in the downstream direction on the axis of symmetry, and along the orifice tip to monitor the pressure field fluctuations and assess the susceptibility to cavitation.

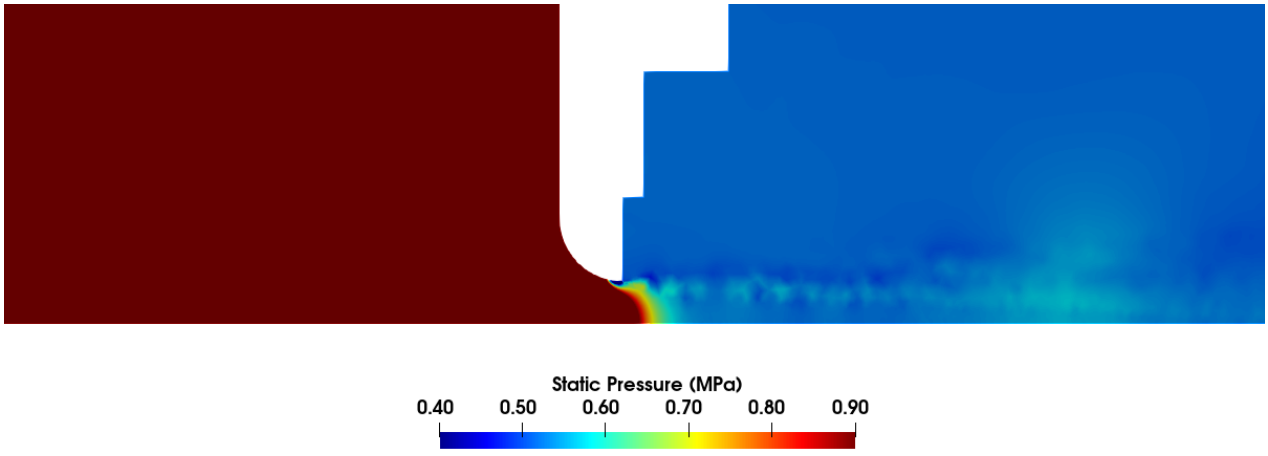

Figure 9: Static pressure field around the orifice at $t = 0.1\ seconds$, showing the region of low pressure around the orifice.

The static pressure contours around the orifice at $t = 0.1$ seconds, are shown in Fig. 9. The pressure falls on the orifice lip surface as the stream lines follow the curvature of its semi-circular geometry, leading to a low pressure point near the tip of the orifice at the orifice exit plane. This is consistent with the previous LES simulation of the orifice nearfield (6) and the pressure gradient contours around the orifice observed in scale resolving simulations.

This highlights another benefit of predicting gas dissolution into the hydraulic oil and its likely distribution within the shock absorber internal domain, as it could significantly improve cavitation modelling by assessing the gas content of oil in areas that are subjected to low pressure under a given loading profile. This is in addition to the aforementioned prediction of gas pressure available to support the aircraft weight.

4 Conclusions

Workflows incorporating multiphysics simulations are a promising area of CFD development that still contain many challenges. Identifying the significant flow physics in a given problem enables efficient and robust implementation of a modular, multi-fidelity framework that facilitates the utilisation of appropriate physics modelling based on the detected flow parameters.

The framework was tested on the internal dynamics of an oleo=pneumatic shock absorber under a drop test loading profile. The main focus was initially on the turbulent flow development and multiphase interaction between hydraulic oil and gas. Conditions for different types of cavitation as well as the severity of multiphase mixing were of particular interest. Multiphase mixing is an important consideration in shock absorber flows because it can significantly increase gas dissolution in oil, which in turn could lead to an unexpected reduction in pneumatic pressure, under strong agitation conditions. This could lead to the shock absorber reaching maximum compression and generating direct contact between internal surfaces. Dissolution of gas in oil can also occur under static conditions due to variations in temperature and pressure, thus increasing the range of potential conditions that should be explored in a design space exploration of such an application. These examples help highlight the importance and advantage of a highly optimised multiphysics framework that accounts for the complexity of the real system as accurately and efficiently as possible.

5 Acknowledgement

This research was funded by Innovate UK grant number 10002411, under the ATI/IUK Project: LANDOne, with Airbus UK as Industrial Lead.

6 Data Availability

The underlying data is available from the DOI: https://doi.org/10.17862/cranfield.rd.24799392 and DOI: https://doi.org/10.17862/cranfield.rd.17701310 which are associated with references (7) and (6), respectively.

References

[1] J. P. Slotnick, A. Khodadoust, J. Alonso, D. Darmofal, W. Gropp, E. Lurie, and D. J. Mavriplis, "Cfd vision 2030 study: a path to revolutionary computational aerosciences," tech. rep., 2014.

[2] F. D. Witherden and A. Jameson, "Future directions in computational fluid dynamics," in 23rd AIAA Computational Fluid Dynamics Conference, no. AIAA 2017-3791, 2017.

[3] D. E. Keyes, L. C. McInnes, C. Woodward, W. Gropp, E. Myra, M. Pernice, J. Bell, J. Brown, A. Clo, J. Connors, et al., "Multiphysics simulations: Challenges and opportunities," The International Journal of High Performance Computing Applications, vol. 27, no. 1, pp. 4–83, 2013.

[4] N. Currey, Aircraft Landing Gear Design: Principles and Practices. AIAA education series, American Institute of Aeronautics and Astronautics, 1988.

[5] R. K. Schmidt, The design of aircraft landing gear. SAE International, 2021.

[6] A. A. Sheikh Al-Shabab, B. Grenko, D. Vitlaris, P. Tsoutsanis, A. F. Antoniadis, and M. Skote, "Numerical investigation of orifice nearfield flow development in oleo-pneumatic shock absorbers," Fluids, vol. 7, no. 2, p. 54, 2022.

[7] A. A. Sheikh Al-Shabab, B. Grenko, P. A. Silva, A. F. Antoniadis, P. Tsoutsanis, and M. Skote, "Unsteady multiphase simulation of oleo-pneumatic shock absorber flow," Fluids, vol. 9, no. 3, p. 68, 2024.

[8] A. A. Sheikh Al-Shabab, D. Vitlaris, Z. Lin, B. Grenko, P. Tsoutsanis, A. Antoniadis, and M. Skote, "Numerical investigation of oleo-pneumatic shock absorber: setup and validation," WCCM-ECCOMAS2020, 2021.

[9] B. Milwitzky and F. E. Cook, "Analysis of landing-gear behavior," NACA Technical Note, no. TN-2755, 1952.

[10] P. A. S. F. Silva, A. A. Sheikh Al-Shabab, P. Tsoutsanis, and M. Skote, "Study of orifice design on oleo-pneumatic shock absorber," Fluids, vol. 9, no. 5, 2024.

[11] F. R. Menter, "Two-equation eddy-viscosity turbulence models for engineering applications," AIAA journal, vol. 32, no. 8, pp. 1598–1605, 1994.

[12] A. A. S. Al-Shabab and P. G. Tucker, "Toward active computational fluid dynamics role in open jet airfoil experiments design," AIAA Journal, vol. 56, no. 8, pp. 3205–3215, 2018.

[13] A. S. Al-Shabab and P. Tucker, "Rans prediction of open jet aerofoil interaction and design metrics," The Aeronautical Journal, vol. 123, no. 1266, pp. 1275–1296, 2019.

[14] N. Solehati, J. Bae, and A. P. Sasmito, "Numerical investigation of mixing performance in microchannel t-junction with wavy structure," Computers & Fluids, vol. 96, pp. 10–19, 2014.

[15] S. Wang, X. Huang, and C. Yang, "Mixing enhancement for high viscous fluids in a microfluidic chamber," Lab on a Chip, vol. 11, no. 12, pp. 2081–2087, 2011.

[16] Q. Nguyen and D. V. Papavassiliou, "Quality measures of mixing in turbulent flow and effects of molecular diffusivity," Fluids, vol. 3, no. 3, p. 53, 2018.

[17] Y. Yan and R. Thorpe, "Flow regime transitions due to cavitation in the flow through an orifice," International journal of multiphase flow, vol. 16, no. 6, pp. 1023–1045, 1990.

[18] S. Osterland, L. Günther, and J. Weber, "Experiments and computational fluid dynamics on vapor and gas cavitation for oil hydraulics," Chemical Engineering & Technology, vol. 46, no. 1, pp. 147–157, 2023.